5⊘CellPress

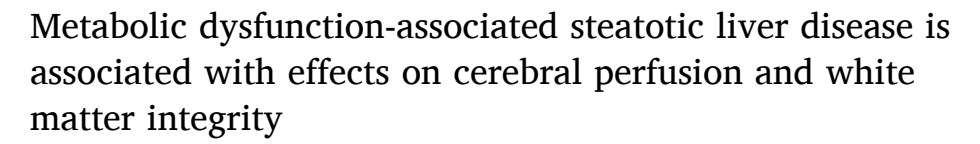
Contents lists available at ScienceDirect

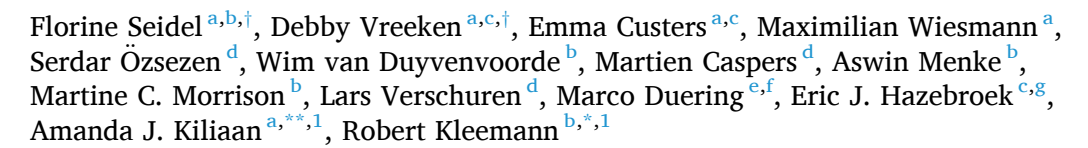
Heliyon

journal homepage: www.cell.com/heliyon



Research article





- ^a Department Medical Imaging, Anatomy, Radboud Alzheimer Center, Donders Institute for Brain, Cognition, and Behavior, Radboud University Medical Center, Geert Grooteplein 21N, 6525 EZ Nijmegen, the Netherlands
- b Department of Metabolic Health Research, Netherlands Organisation for Applied Scientific Research (TNO), Sylviusweg 71, 2333 BE Leiden, the Netherlands
- ^c Department of Bariatric Surgery, Vitalys, part of Rijnstate hospital, Postbus 9555, 6800 TA Arnhem, the Netherlands
- ^d Department of Microbiology and Systems Biology, Netherlands Organisation for Applied Scientific Research (TNO), Sylviusweg 71, 2333 BE Leiden, the Netherlands
- e Institute for Stroke and Dementia Research (ISD), University Hospital LMU Munich, Feodor-Lynen-Straße 17, 81377 Munich, Germany
- ^f Medical Imaging Analysis Center (MIAC) and Department of Biomedical Engineering, University of Basel, Marktgasse 8, CH-4051 Basel, Switzerland
- g Division of Human Nutrition and Health, Wageningen University, Postbus 17 6700 AA Wageningen Wageningen, the Netherlands

ARTICLE INFO

Keywords: MASLD Metabolism Brain health Systemic inflammation

ABSTRACT

It is unclear whether early metabolic and inflammatory aberrations in the liver are associated with detrimental changes in brain structure and cognitive function. This cross-sectional study examines putative associations between metabolic dysfunction-associated steatotic liver disease (MASLD) and brain health in 36–55 year-old participants with obesity (n=70) from the BARICO study (BAriatric surgery Rijnstate and Radboudumc neuroImaging and Cognition in Obesity). The participants underwent brain magnetic resonance imaging to study brain volumes and cortical thickness (3T MRI including T1-weighted magnetization-prepared rapid gradient-echo sequence), cerebral blood perfusion (arterial spin labeling) and white matter integrity (diffusion weighted

Abbreviations: ANGPTL4, angiopoietin-like 4; AhR, Aryl Hydrocarbon Receptor Signaling; ApoB100, Apolipoprotein B100; BMI, body mass index; BS, bariatric surgery; CBF, cerebral blood flow; CI, confidence interval; CRP, C-reactive protein; CE, cholesteryl esters; COWAT, Controlled Oral Word Association Test; CSVD, cerebral small vessel disease; DAG, diacylglycerols; FC, free cholesterol; GM, grey matter; ICV, intracranial volume; LPS-BP, LPS-binding protein; MASLD, metabolic dysfunction-associated steatotic liver disease; MD, mean diffusivity; MoCA, Montreal Cognitive Assessment; MRI, magnetic resonance imaging; NAcc, nucleus accumbens; NGS, next generation sequencing; PVC, partial volume correction; sCoV, spatial coefficient of variation; TAP, Tests of Attentional Performance; TNF-α, tumor necrosis factor α; TG, triglycerides; WC, waist circumference; WM, white matter; WMH, white matter hyperintensities.

- * Corresponding author. Sylviusweg 71, 2333 BE Leiden, the Netherlands.
- ** Corresponding author. Geert Grooteplein 21N, 6525 EZ Nijmegen, the Netherlands.
 - E-mail addresses: Amanda.kiliaan@radboudumc.nl (A.J. Kiliaan), Robert.kleemann@tno.nl (R. Kleemann).
- † Florine Seidel and Debby Vreeken contributed equally to this work as first authors.
- $^{\mathrm{1}}$ Amanda J. Kiliaan and Robert Kleemann contributed equally to this work as senior authors.

https://doi.org/10.1016/j.heliyon.2024.e38516

Received 4 April 2024; Received in revised form 29 August 2024; Accepted 25 September 2024 Available online 26 September 2024

2405-8440/© 2024 The Authors. Published by Elsevier Ltd. This is an open access article under the CC BY-NC-ND license (http://creativecommons.org/licenses/by-nc-nd/4.0/).

imaging to assess mean-skeletonized mean diffusivity and fluid-attenuated inversion recovery to detect the presence of white matter hyperintensities (WMH)). The participants additionally performed neuropsychological tests to assess global cognition, working and episodic memory, verbal fluency and the ability to shift attention. Liver biopsies were collected and liver dysfunction was examined with histopathological, biochemical, and gene expression analyses. Linear regression analyses were performed between liver and brain parameters and the influence of body-mass index, diabetes and hypertension was explored. Early stages of liver disease were not associated with cognitive status but with cerebrovascular changes independently of age, sex, BMI, diabetes and hypertension: hepatic fibrosis development was associated with higher spatial coefficient of variation (sCoV) in the nucleus accumbens (NAcc), reflecting greater variations in cerebral perfusion and reduced vascular efficiency. Elevated hepatic levels of free cholesterol and cholesteryl esters were associated with increased WMH, indicating cerebral small vessel disease. RNA-seq and pathway analyses identified associations between sCoV in NAcc and WMH and the expression of hepatic genes involved in inflammation and cellular stress. Additionally, sCoV in NAcc correlated with plasma IL-6 levels suggesting that systemic-low grade inflammation may, at least partly, mediate this relationship. In conclusion, this study demonstrates that specific features of liver dysfunction (e.g. free cholesterol, onset of fibrosis) are associated with subtle cerebrovascular impairments, when changes in cognitive performance are not yet noticeable. These findings highlight the need for future research on therapeutic strategies that normalize metabolicinflammatory aberrations in the liver to reduce the risk of cognitive decline.

1. Introduction

Obesity is increasingly linked to detrimental changes in brain structure and cognitive performance [1]. For instance, a high body mass index (BMI) has been associated with reduced grey matter (GM) volumes and cortical thickness [2–4], which are often accompanied by an impaired cerebral blood flow (CBF) [5]. Additionally, obesity has been linked to increased white matter (WM) lesions [2,6], visible as abnormal areas of signal intensity (WM hyperintensities, WMH) on magnetic resonance imaging (MRI) and established as indicators of cerebral small vessel disease (CSVD) [7]. WM integrity can further be assessed by diffusion-weighted imaging in which mean diffusivity (MD) in WM is associated with cognitive decline in multiple cognitive domains [8], but the findings are still inconsistent [9]. Middle-aged adults with obesity often exhibit poorer cognitive performance, particularly in memory and executive function (reviewed in Ref. [1]).

Despite numerous studies showing negative associations between obesity and brain health, the underlying biological processes remain poorly understood. Dysfunction of the liver, a key organ in energy metabolism and metabolic homeostasis [10], has been proposed to be implicated in these relationships. Indeed, several studies have shown that people with metabolic dysfunction-associated steatotic liver disease (MASLD), exhibit reduced brain volumes [11,12] and altered CBF [13]. Recent studies also provided evidence for associations between impaired liver function and decreased brain volumes and blood perfusion, already at early liver disease stages [14]. Advanced MASLD-related fibrosis was further associated with increased WMH [15]. In addition, MASLD has been associated with poorer cognitive function but this association seems to depend on the cognitive domains investigated (reviewed in Ref. [16]). However, these findings rely mostly on non-invasive examination of the livers (e.g. ultrasound, computed tomography, blood markers) or categorical information on liver histology while associations on a more granular (molecular) level between processes in the liver and brain health are still largely unknown.

The present study therefore combines histological, biochemical and molecular (-omics) profiling of liver biopsies with comprehensive neuroimaging to investigate the relationship between early MASLD disease processes and brain health in obesity. Liver biopsies were obtained from participants in the BARICO study (BAriatric surgery Rijnstate and Radboudumc neuroImaging and Cognition in Obesity) who were eligible for bariatric surgery (BS) [17]. The livers were histologically and biochemically analyzed to distinguish interindividual differences in liver histopathology, hepatic lipid content, gene expression and biological pathway activation. The participants underwent brain MRI providing detailed insights into brain structure and perfusion: brain volumes (structural data) and cerebral perfusion were analyzed in multiple cortical and sub-cortical regions, and WM integrity was assessed by mean-skeletonized mean diffusivity (MSMD) and WMH content. Complementary neuropsychological tests were performed to assess global cognition, working and episodic memory, verbal fluency and the ability to shift attention. Associations between liver dysfunction and brain health were investigated using linear regression models, which also allowed us to explore the effects of BMI, hypertension and diabetes in these relationships. This study highlights the importance of investigating the onset of obesity-associated changes in the brain, and underscores the need to develop therapeutic strategies that improve whole-body metabolic homeostasis.

2. Methods

2.1. Study population and tissue samples

This study used liver biopsies, plasma samples and MRI data from the BARICO study [17,18]. The primary aim of the BARICO study was to longitudinally investigate the short and long-term effects of weight loss after bariatric surgery on brain structure and function

using brain MRI and neuropsychological tests. As a secondary endpoint, the BARICO study aimed to investigate the relationship between the metabolic and inflammatory status of the liver, white adipose tissue and gut, and brain structure and function in obesity (i. e. before bariatric surgery). The BARICO study was approved by the medical review ethics committee CMO Region Arnhem and Nijmegen (NL63493.091.17) and prospectively registered in the Dutch Trial Registry [19]. The study was conducted in compliance with the Declaration of Helsinki 'Ethical Principles for Medical Research Involving Human Subjects' and the guidelines for Good Clinical Practice (CPMP/ICH/135/95). Written informed consent was obtained from each participant included in the study. 156 people eligible for BS (35–55 years old, BMI ≥30) were recruited between September 2018 and December 2020 at the Rijnstate Hospital (Arnhem, the Netherlands) and data were collected from September 2018 and March 2021. Inclusion criteria included the eligibility to undergo Roux-en-Y gastric bypass for morbid obesity and an age between 35 and 55 years old. The participants undergoing brain MRI needed to be right handed. General exclusion criteria included previous or current neurological or severe psychiatric illness, pregnancy, the use of any antibiotic, probiotic, or prebiotic agent three months before or during the study (excluding preoperative prophylaxis). Additional exclusion criteria for the participants undergoing brain MRI included claustrophobia, epilepsy, lying circumference above the MRI space, color blindness as well as the presence of pacemakers and defibrillators, nerve stimulators, intracranial clips, infraorbital or intraocular metallic fragments, cochlear implants, ferromagnetic implants. Brain MRI, neuropsychological tests and fasted blood collection were performed on a subset of 76 subjects 4–8 weeks before BS.

During medical examinations, anthropometric characteristics, clinical chemistry (including total cholesterol, HDL-cholesterol, and LDL-cholesterol levels), diabetes and hypertension were determined as previously described [18]. Of note, waist circumference (WC) could not be measured in all individuals of the BARICO study due to restrictions during the Covid-19 pandemic. This affected 10 individuals from the subset of patients included in the present study. Diabetes was defined as the use of antidiabetic drugs or insulin and/or fasting blood glucose \geq 7.0 mmol/L and plasma HbA1c \geq 48 mmol/mol. Hypertension was defined as the use of anti-hypertensive medication and/or blood pressure \geq 130/80 mmHg. 50 % of the participants did not consume alcohol. For the other participants, alcohol consumption was occasional (between 0 and 8 glasses per week).

Wedge liver biopsies were obtained from 70 MRI participants during BS. Causes for missing liver biopsies included too high risk of bleeding, or absence of specific consent. The present study concentrates on the 70 subjects who donated liver biopsies and their corresponding brain datasets (Supplementary Fig. S1). An overview of the general characteristics of the participants included in this study are provided in Table 1.

2.2. MRI procedures

Brain MRI was performed using a 3T Magnetom Skyra scanner (Siemens Healthineers, Erlangen, Germany) with a 32-channel head coil. All MRI procedures and image processing are extensively described elsewhere [18]. An overview of the brain readouts and averages is provided in Table 2.

2.2.1. Structural data

A T1-weighted 3D magnetization-prepared rapid gradient-echo sequence (repetition time (TR): 2300 ms; inversion time (TI): 1100 ms; echo time (TE): 3.03 ms; 8° flip angle; voxel size: 1 mm isotropic) was performed for anatomical reference and macroscopic brain structure analysis. Brain volume and cortical thickness were determined by volumetric segmentation and cortical reconstruction using FreeSurfer Imaging Analysis Suite (v.6.0.0, http://surfer.nmr.mgh.harvard.edu/) [20]. The volume of brain regions were measured based on combined structural atlases [21,22] and expressed as percentage of intracranial volume (ICV) (based on estimated total

Table 1General characteristics of the participants undergoing brain MRI.

	$\text{Mean} \pm \text{SD}$	Range
Age (years)	45.0 ± 5.8	[36.2–55.2]
Sex (% women)	82.9 %	
Height (m)	1.70 ± 0.07	[1.57–1.89]
Weight (kg)	118.4 ± 14.5	[95.4–159.0]
BMI (kg/m2)	40.7 ± 3.8	[34.7–52.9]
Waist circumference (cm)	122.2 ± 10.5	[101-150]
Smoking (% participants)	13.1 %	
Alcohol consumption (% participants)	50.0 %	
Education		
Low (scores 1-4) (% participants)	11.6 %	
Middle (score 5) (% participants)	52.2 %	
High (scores 6-7) (% participants)	36.2 %	
Comorbidities		
Diabetes mellitus (% participants)	17.1 %	
Glucose (mmol/l)	6.5 ± 2.8	[4.4–18.4]
HbA1C (mmol/mol)	40.5 ± 11.8	[30.0-89.0]
Hypertension (% participants)	64.3 %	
Systolic blood pressure (mmHg)	134.9 ± 16.1	[105-184]
Diastolic blood pressure (mmHg)	84.5 ± 8.8	[66-113]

Only subjects with liver biopsies are included (n = 70).

Table 2Brain MRI characteristics of the participants.

Brain into characteristics of the participants.	
Brain parameter	$Mean \pm SD$
Cognition	
z-score	0.02 ± 0.63
Digit span	26.57 ± 5.15
Story recall	16.65 ± 7.1
TAP score	-0.79 ± 6.83
Verbal fluency	37.7 ± 10.51
MoCA	26.77 ± 2.66
Brain volumes (%ICV)	
GM	40.21 ± 3.33
WM	30.82 ± 2.98
Frontal cortex	10.49 ± 0.98
Parietal cortex	7.19 ± 0.75
Temporal cortex	6.32 ± 0.63
Occipital cortex	2.81 ± 0.35
Cingulate gyrus	1.20 ± 0.11
Insula	0.85 ± 0.08
Putamen	0.65 ± 0.07
NAcc	0.06 ± 0.01
Caudate nucleus	$\textbf{0.47} \pm \textbf{0.06}$
Hippocampus	0.56 ± 0.05
Amygdala	0.23 ± 0.02
Cortical thickness (mm)	
Overall cortical thickness	2.45 ± 0.08
Frontal cortex	2.55 ± 0.10
Parietal cortex	2.39 ± 0.09
Temporal cortex	2.71 ± 0.09
Occipital cortex	1.94 ± 0.09
Cingulate gyrus	2.39 ± 0.08
Insula	2.89 ± 0.10
CBF (ml/100g tissue/min)	
GM	46.32 ± 8.83
Frontal cortex	47.67 ± 10.49
Parietal cortex	51.34 ± 10.19
Temporal cortex	52.58 ± 9.45
Occipital cortex	51.3 ± 11.23
Cingulate gyrus	49.09 ± 10.23
Insula Putananan	47.47 ± 9.11
Putamen	38.29 ± 9.36
NAcc	36.06 ± 14.56 35.52 ± 10.16
Caudate nucleus	35.52 ± 10.16
sCoV (%) GM	4.37 ± 1.41
Frontal cortex	4.17 ± 1.69
Parietal cortex	5.46 ± 1.67
Temporal cortex	4.76 ± 1.25
Occipital cortex	6.44 ± 2.36
Cingulate gyrus	3.34 ± 0.85
Insula	3.36 ± 1.15
Putamen	3.06 ± 3.19
NAcc	5.63 ± 4.07
Caudate nucleus	4.23 ± 1.70
MSMD	3.39 ± 0.11
WMH volume	0.34 ± 0.66
WMH number	10 ± 18

Only subjects with liver biopsies are included (n = 70). Data are expressed as mean \pm SD. Abbreviations: (ICV) intracranial volume; (CBF) cerebral blood flow; (GM) grey matter; (MSMD) mean skeletonized mean diffusivity; (NAcc) nucleus accumbens; (sCoV) spatial coefficient of variation; (WM) white matter; (WMH) WM hyperintensities.

intracranial volume (eTIV) calculated with FreeSurfer). These regions included total GM and WM and cortical regions (frontal, parietal, temporal and occipital cortices). In addition, we examined the cingulate gyrus involved in emotion and behavior regulation and decision-making [23], and the insula involved in sensory processing, emotions and empathy, gustatory and sensorimotor processing, taste perception, and decision-making [24], knowing that obesity is linked to disturbances in both regions [25,26]. We further examined components of the basal ganglia (caudate nucleus, putamen) and nucleus accumbens (NAcc), all being involved in a wide range of cognitive functions including motor control, decision-making, reward processing, emotional behaviors, executive functions,

and habit formation [27]. Previous studies notably showed that obesity can trigger structural and functional alterations in networks involving the basal ganglia and NAcc which were further linked to reward system and inhibitory control [28]. We also looked at the amygdala, part of the brain's limbic system playing a crucial role in processing emotions, particularly fear and anxiety, but also affecting feeding behavior [29,30]. We finally studied the hippocampus, a key structure involved in memory [31]. Overall cortical thickness and thickness of the aforementioned cortical regions were determined (in mm). Scans of poor quality were excluded from the structural dataset (n = 3).

2.2.2. Cerebral blood perfusion

CBF (ml/100 g/min) was measured in overall GM and individual brain regions (i.e. frontal, parietal, temporal and occipital cortices, cingulate gyrus, insula, putamen, NAcc and caudate nucleus) using a pulsed arterial spin labeling sequence (PICORE, bolus duration: 700 ms; TI: 1800 ms) with 2D echo-planar imaging readout (TR: 2500 ms; TE: 12 ms; voxel size: 4 × 4 mm, 9 slides of 8 mm with a 2-mm slice gap, 45 control-label pairs, no background suppression, mean control used as M0). Processing of arterial spin labeling images was performed using Matlab (version 2020a, MathWorks, MA) and the toolbox ExploreASL (version 1.5.1, [32]), including SPM 12 (version 7219, Statistical Parametric Mapping, Wellcome Trust Centre for Neuroimaging, London, United Kingdom), CAT12 (version r1615), and LST (version 2.0.15) as previously described [18]. ExploreASL notably employs partial volume correction (PVC) technique [32]. We specifically used the ROI-based PVC method, known as the 'Asllani method', which is a two-component regression approach [33]. This method does not involve a threshold on GM partial volume but rather separates the contributions of GM and WM to the measured signal. Quality control was performed using ExploreASL's integrated quality control parameters, which include visual inspection of unmasked images in standard space and comparison with an atlas, group average, or previous study to detect technical failures, outliers, and artifacts [32]. Whole-brain and regional differences larger than 2-3 SD were visually inspected, and deviations were noted. ExploreASL further uses an adaptation of the SPM12 motion correction to minimize apparent motion attributable to the control-label intensity difference from the estimated motion parameters via a 'zig-zag' regressor [32,34]. Scans of subjects presenting excessive head motion were excluded (n = 5). Corresponding spatial coefficients of variation (sCoV, %) were calculated as the standard deviation divided by mean CBF [35]. sCoV is a parameter that reflects the variability in CBF, with higher sCoV values indicating greater variability in CBF and potentially reduced vascular efficiency (i.e. impaired distribution of blood and oxygen) [35].

2.2.3. WMH and MSMD

As an indicator of CSVD, WMH of presumed vascular origin [7] were segmented using a fully automated, deep-learning algorithm based on multi-dimensional gated recurrent units with 3D fluid-attenuated inversion recovery (FLAIR) sequence (TR: 5000 ms; TI: 1800 ms; TE: 397 ms; 120° flip angle; voxel size: 1 mm isotropic) and 3D T1-weighted images as input [36]. Quality assessment was conducted through visual inspection. Output segmentation masks were used to determine WMH count and volume. WMH data were missing for two subjects due to logistical issues during scanning.

WM integrity was further assessed by MD in the main WM tracts, known to be associated with performance in multiple cognitive domains [9]. MSMD was calculated based on multidirectional diffusion weighted imaging (DWI) data using a multiband echo-planar imaging (TR: 3275 ms; TE: 91.4 ms; voxel size: 1.9 mm isotropic; $6 \times b = 0 \text{ s/mm}^2$, $42 \times b = 900 \text{ s/mm}^2$, $83 \times b = 1800 \text{ s/mm}^2$) and a publicly available pipeline script (https://github.com/miac-research/psmd, version 1.5 (2019)). DWI data were processed using Functional Magnetic Resonance Imaging of the Brain software library (FSL; v6.0.1, [37]) as previously described in detail [18]. Quality was controlled using the FSL eddy tool Quality Assessment for DWI (eddy_quad) and visual inspection the images. Scans with poor quality were excluded and one participant had no DWI scan due to time issues (n = 5 missing in total).

2.3. Cognitive performance

Education levels were determined using the Verhage score based on the Dutch education system [38]. Cognitive performance was assessed as extensively described previously [18]. Montreal Cognitive Assessment (MoCA) was first used to evaluate general cognitive performance. Working memory was assessed using the three added scores (forward, backward, sorting) of the Digit Span test (Wechsler Adult Intelligence Scale-Fourth Edition [39]. Episodic memory was examined using the added scores of the immediate and delayed Story Recall test (from Rivermead Behavioral Memory test) [40]. Verbal fluency was assessed using the total score of Controlled Oral Word Association Test (COWAT) [41]. The ability to shift attention was finally determined with the Flexibility subtest score from the computerized Tests of Attentional Performance (2.3, TAP) [42]. In parallel, as an indication of global cognition, a compound z-score was calculated as the average of the z-scores of the individual tests. These individual z-scores were calculated as the raw score minus the population mean, divided by the population standard deviation [18,43].

2.4. Analyses of liver biopsies

2.4.1. Liver histology

A portion of each liver biopsy was fixed in 4 % paraformaldehyde for 36–48 h, dehydrated overnight (Automatic Tissue Processor ASP300S, Leica Biosystems, Amsterdam, the Netherlands) and embedded in paraffin. 3 μ m-thick cross-sections were prepared and stained with hematoxylin-eosin or Sirius Red (Automated Slide Stainer, ST5010, Leica). NAFLD activity scores (NAS) were determined by a board-certified pathologist according to the scoring system of Kleiner et al. (i.e. unweighted sum (0-18) of the scores for steatosis (0–7), inflammation (0–6), and liver injury (0–5) [44] and the scoring system of Hjelkrem et al. (i.e. sum of the scores for steatosis

(0–3), lobular inflammation (0–3), and ballooning (0–2) [45]. The scores per participant are provided in Supplementary Table S1. To perform linear regression we used continuous values, i.e. the absolute percentages of steatosis (both macrovesicular and microvesicular) and fibrosis, and the absolute counts of inflammatory aggregates as described previously by Liang et al. [46]. More specifically, macrovesicular and microvesicular steatosis were determined as the percentage of liver tissue affected at 50× magnification and the total steatosis was calculated as the sum of macrovesicular and microvesicular steatosis. Inflammation was assessed as the number of inflammatory cell aggregates per cm² at 100× magnification. 4–5 non-overlapping fields were used per sample and periportal inflammatory aggregates were excluded. Fibrosis was determined as the percentage of Sirius Red-positive area.

2.4.2. Liver lipid analysis

Another portion of each liver biopsy was snap-frozen in liquid nitrogen and stored at $-70\,^{\circ}$ C. Liver homogenates were prepared using a bead-beater and protein content was determined by Lowry protein assays. To further characterize lipid accumulation in the liver, intrahepatic contents of triglycerides (TG), cholesteryl esters (CE) and free cholesterol (FC) were quantified with high-performance thin layer chromatography (HPTLC) as reported previously [47]. In an independent analysis, liver diacylglycerols (DAG) were quantified in the liver homogenates with DAG Assay Kit (ab242293, Abcam, Cambridge, UK) according to manufacturer's instructions.

2.4.3. Liver next-generation sequencing (NGS)

RNA was extracted from ~ 10 mg snap-frozen liver tissue using a total-RNA isolation kit (Bio-connect, Huissen, the Netherlands) as described previously [47,48]. RNA concentrations were determined using Nanodrop 1000 (Isogen Life Science, De Meern, the Netherlands) and RNA integrity was assessed using RNA 6000 Nano LabChip 669 kit and a bioanalyzer 2100 (Agilent Technologies, Amstelveen, the Netherlands). NGS (NovaSeq6000) was performed at GenomeScan (Leiden, the Netherlands). The transcriptomics dataset of this study can be found in the Gene Expression Omnibus (GEO) repository (https://www.ncbi.nlm.nih.gov/gds). Ribosomal RNA (rRNA) was depleted from total RNA using an rRNA depletion kit (NEB#E6310). After fragmentation of rRNA-depleted RNA, cDNA synthesis was performed and used for ligation with sequencing adapters and PCR amplification of the resulting products. The fastq sequencing data (~40 Mreads/sample) was trimmed, mapped to the human genome (Homo sapiens.GRCh38.gencode.v29) and counted (#reads/gene). RNA-seq data of n = 1 subject was an outlier in several unsupervised methods (PCA, MDS, Distance matrix, Clustering) and was excluded as a technical outlier. For normalization, mRNA raw counts were first transformed into sample-normalized counts (nCnts) by dividing all raw counts per gene (rCnts) by its sample total counts (totCnts): nCnts = rCnts/totCnts. Next, an arbitrary reference group was defined based on the histological criteria: <3.5 % steatosis of surface area, <35 inflammatory aggregates per cm², ≤ 1 % fibrosis, no periportal or pericentral fibrosis. N = 11 livers from the complete BARICO trial fulfilled these criteria. nCnts were then divided by the average nCnts from the arbitrary reference group for each gene. This 'double' normalized gene expressions were correlated (Pearson ranked) with brain readouts. The significantly correlating genes (using correlation p-values <0.01) were evaluated by pathway gene enrichment analyses ([47], Ingenuity Pathway Analysis software, v.81348237, Qiagen, Redwood City, USA), resulting in p-values ranked canonical pathways and upstream regulators pathways.

2.5. Plasma analyses

Biomarkers were measured in plasma using ELISAs, from R&D systems (Minneapolis, USA): high sensitive C-reactive protein (CRP, #DY1707), LPS-binding protein (LPS-BP, #DY870-05) and angiopoietin-like 4 (ANGPTL4, #DY3485), from Novus Biologicals (Littleton, USA): complement component 3 and 5 (#NBP2-60618 and #NBP2-606205), from ThermoFisher Scientific (Loughborough, UK): Apolipoprotein B100 (ApoB100, #EH35RB), or by a multiplex SP-XTM imaging system from Quanterix (Billerica, USA): IL-1 β and IL-6. Bile acid profiling analysis was performed at Triskelion (Utrecht, the Netherlands) and data were expressed as μ mol bile acids/1 of plasma as described elsewhere [49]. In addition, the concentrations of hydrolyzed fatty acids were determined in corresponding red blood cells samples at OmegaQuant Analytics (Sioux Falls, SD, USA) as described [50]. The total saturated (SFAs), monounsaturated (MUFAs), polyunsaturated (PUFAs) and trans-unsaturated (trans-FAs) fatty acid contents in red blood cells were determined (in μ g/mg). Omega-3 index was calculated as the sum of eicosapentaenoic acid (EPA) and docosahexaenoic acid (DHA) concentrations divided by the total fatty acid concentration. Five plasma/red blood cell samples were not included in this analysis because insufficient plasma was available.

2.6. Statistical analyses

To compare general characteristics between men and women, independent t-tests (two-tailed) were performed for normally-distributed variables and non-parametric Kruskal-Wallis was used if normality assumption was not met. SPSS software (version 28, IBM, Armonk, USA) was used and differences were considered statistically significant for p-value (P) \leq 0.05. Hematocrit values and head motion for sCoV and CBF, and head motion for MSMD were tested as potential covariates using Pearson correlations. As these variables were not associated with GM sCoV, GM CBF or MSMD (P) the following analyses were not adjusted for hematocrit values and head motion. In a second step, relationships between liver histology, liver lipid contents, plasma and red blood cells parameters and brain parameters were investigated with linear regressions using SPSS [18]. Two models of linear regressions were used: a 'Crude mode' with no adjustments and a 'Full model' that included adjustments for age, sex, smoking, alcohol consumption and education. To evaluate whether the observed relationships were influenced by BMI and metabolic comorbidities, additional models were performed: Full model + BMI: adjustment of full model + BMI; Full model + T2DM: adjustment of full model + diabetes; Full

model + HT: adjustment of full + hypertension. An additional model adjusted for WC(Full model + WC) was explored and reported textually. It is however important to consider that due to missing WC data for 10 individuals (Covid-19 pandemic), the power of this explorative analysis is lower. Associations were considered significant when $P \le 0.01$, and data are expressed as unstandardized β coefficient with confidence interval. As this study explores potential relationships between liver and brain health (hypothesis-generating approach), no correction for multiple comparison was used. In addition, the exploratory relationships between hepatic gene expression and brain MRI were assessed by Pearson correlations using Microsoft Excel (Version 2023, Redmond, USA). For this analysis, sCoV in NAcc and WMH count were used as brain MRI parameters since they significantly correlated with liver parameters in both Crude and Full models. The statistical threshold for pathway enrichment and upstream regulator analyses was set at $P \le 0.01$ per pathway.

3. Results

3.1. Study population characteristics

3.1.1. General characteristics

The general characteristics of the 70 MRI participants who donated liver biopsies and the corresponding population average for each brain MRI parameter measured are respectively displayed in Tables 1 and 2. Their age range was 36–55 years with an average BMI of $40.7 \pm 5.8 \text{ kg/m}^2$ 17 % of the participants had diabetes and 64 % had hypertension. 83 % of the participants was female. The men were on average older and had greater height, weight, and WC than the women (Supplementary Table S2). A larger proportion of the men regularly consumed alcohol and had hypertension.

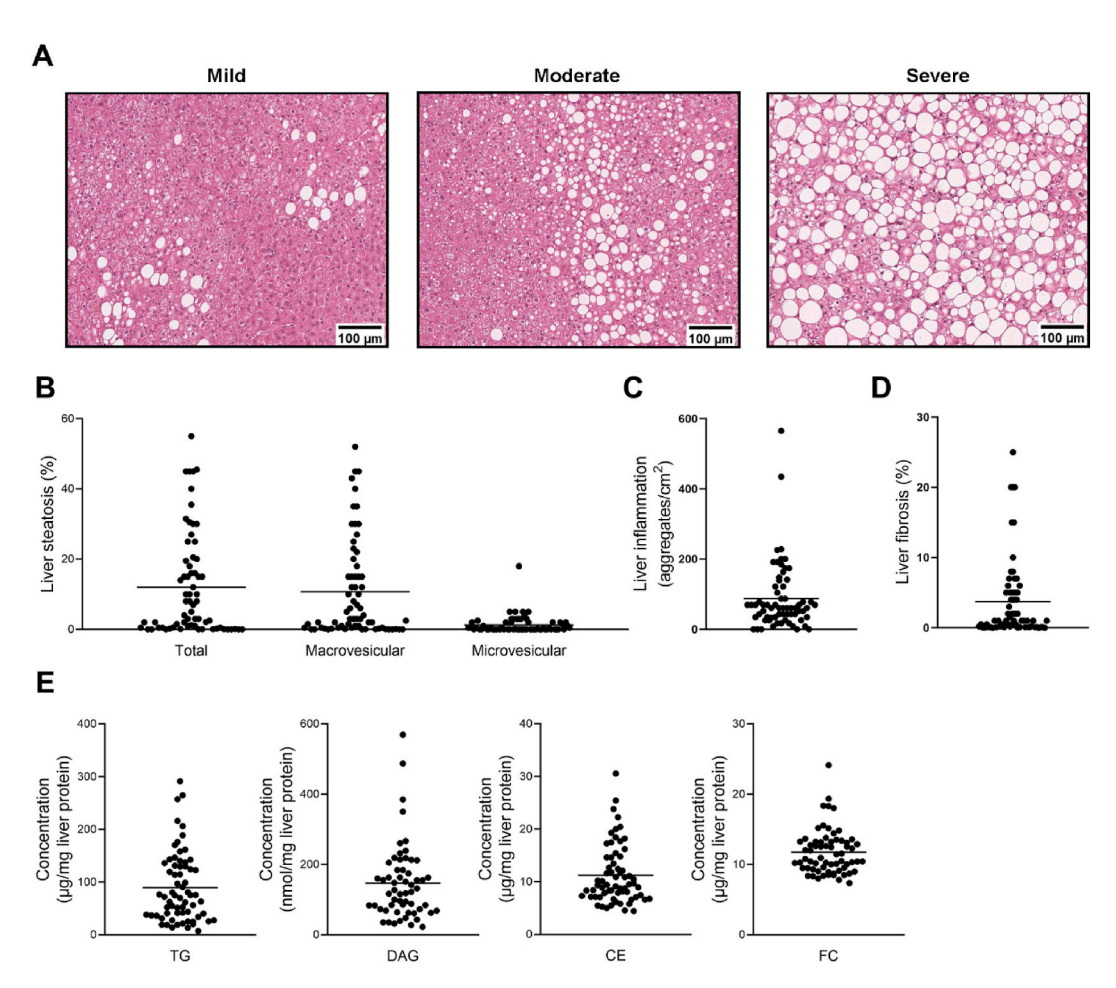


Fig. 1. Variation in liver steatosis and intrahepatic lipids between the participants. (A) Representative photomicrographs of mild, moderate, and severe liver steatosis in patients undergoing brain MRI. (B) Liver steatosis, (C) liver inflammation, (D) liver fibrosis and (E) liver lipids. Each dot represents one subject and the black line indicates the mean. Abbreviations: (DAG) diacylglycerols, (CE) cholesteryl esters, (FC) free cholesterol, (TG) triglycerides.

3.1.2. Liver characteristics

Histopathological analyses of liver biopsies revealed that most patients had some degree of steatosis with pronounced interindividuals variations (Fig. 1A–B). On average 12.0 ± 14.6 % of the cross-sectional area was steatotic, with macrovesicular steatosis being the prevailing form as expected. The livers showed varying degrees of lobular inflammation and fibrosis with on average 87.6 ± 95.4 inflammatory aggregates/cm² and 3.7 ± 5.6 % Sirius Red-positive cross-sectional area (Fig. 1C–D) indicating that the level of inflammation and fibrosis was low to modest. Subsequent biochemical analysis of liver lipid content demonstrated pronounced interindividual variations in hepatic TG, CE, FC and DAG (Fig. 1E–F).

3.2. Liver fibrosis is associated with poorer NAcc perfusion

To investigate potential relationships between liver and brain health, linear regressions were performed between liver histology and brain MRI and cognitive performance. Significant associations are displayed in Table 3 and all linear regressions with corresponding confidence intervals are available in Supplementary Table S3. No significant associations were found between liver histology and cognitive performance, except a very slight positive association between liver inflammation and compound z-score when the Full model was additionally adjusted for WC ($\beta = 0.096$, P = 0.008, CI (95 %) = [0.026; 0.165], not shown). As mentioned earlier, the sample size was lower for this model due to missing WC data (~20 % less). Higher microvesicular steatosis, but not total or macrovesicular steatosis, was associated with larger frontal cortex and putamen in all models except the crude model. Microvesicular steatosis was also associated with GM and parietal cortex volumes when the association was additionally adjusted for BMI. Liver inflammation was not associated with any brain parameters. Increased liver fibrosis was associated with increased NAcc sCoV – reflecting higher variation in NAcc perfusion (lower vascular efficiency) – in all models, including models additionally adjusted for BMI, diabetes or hypertension.

Table 3Significant associations between liver histology and brain parameters.

Brain parameter	Total steatosis		Macrovesicular steatosis		Microvesicular steatosis		Inflammation		Fibrosis	
	β	P	β	P	β	P	β	P	β	P
Brain volumes										
GM										
Crude model	-0.013	0.659	-0.024	0.422	0.295	0.073	0.238	0.216	-0.100	0.184
Full model	0.020	0.517	0.006	0.849	0.376	0.019	0.226	0.227	-0.169	0.021
Full model + BMI	0.022	0.495	0.007	0.842	0.491	0.006	0.224	0.237	-0.168	0.024
Full model + T2DM	0.019	0.570	0.003	0.921	0.373	0.021	0.224	0.252	-0.170	0.022
$Full\ model + HT$	0.016	0.613	0.003	0.935	0.352	0.030	0.219	0.241	-0.167	0.022
Frontal cortex										
Crude model	-0.004	0.640	-0.008	0.364	0.107	0.027	0.061	0.286	-0.026	0.250
Full model	0.006	0.511	0.001	0.905	0.131	0.006	0.058	0.301	-0.044	0.045
Full model + BMI	0.007	0.473	0.001	0.892	0.176	0.001	0.057	0.318	-0.044	0.051
Full model + T2DM	0.007	0.474	0.002	0.872	0.133	0.006	0.064	0.272	-0.044	0.048
Full model + HT	0.005	0.596	0.000	0.983	0.126	0.009	0.056	0.318	-0.044	0.048
Parietal cortex										
Crude model	0.001	0.927	-0.001	0.874	0.050	0.180	0.051	0.239	-0.016	0.340
Full model	0.011	0.104	0.009	0.210	0.074	0.036	0.053	0.193	-0.034	0.035
Full model + BMI	0.012	0.092	0.009	0.207	0.100	0.010	0.052	0.206	-0.033	0.040
Full model + T2DM	0.011	0.123	0.009	0.245	0.073	0.040	0.052	0.225	-0.034	0.035
Full model + HT	0.011	0.125	0.009	0.237	0.071	0.047	0.052	0.204	-0.034	0.037
Putamen										
Crude model	0.001	0.137	0.001	0.281	0.008	0.011	0.007	0.058	-0.002	0.191
Full model	0.001	0.033	0.001	0.109	0.010	0.003	0.008	0.052	-0.003	0.053
Full model + BMI	0.001	0.043	0.001	0.117	0.010	0.006	0.008	0.044	-0.003	0.041
Full model + T2DM	0.001	0.050	0.001	0.158	0.010	0.004	0.007	0.077	-0.003	0.049
Full model + HT	0.001	0.038	0.001	0.121	0.010	0.004	0.008	0.055	-0.003	0.056
sCoV										
NAcc										
Crude model	-0.040	0.273	-0.038	0.321	-0.151	0.469	-0.151	0.533	0.329	0.000
Full model	-0.041	0.301	-0.041	0.318	-0.053	0.795	-0.103	0.664	0.295	0.001
Full model + BMI	-0.042	0.290	-0.041	0.319	-0.088	0.701	-0.100	0.675	0.295	0.001
Full model + T2DM	-0.033	0.421	-0.033	0.441	-0.038	0.853	-0.049	0.842	0.298	0.001
Full model + HT	-0.041	0.308	-0.041	0.326	-0.050	0.811	-0.102	0.669	0.295	0.001

Results of linear regressions: Crude model: no adjustments; Full model: adjustment for age, sex, smoking, alcohol consumption and education; Full model + BMI: adjustment of full model + BMI: adjustment of full model + T2DM: adjustment of full model + diabetes; Full model + HT: adjustment of full model + hypertension. Full model + WC was additionally and exploratively tested and significant associations were similar to the ones observed in the Full model, except for a slight positive association between liver inflammation and the compound-z-score (β = 0.096, P = 0.008, CI (95 %) = [0.026; 0.165]). Significant associations (P \leq 0.01) are indicated in bold. Abbreviations: (GM) grey matter; (NAcc) nucleus accumbens, (sCoV) spatial coefficient of variation.

3.3. Intrahepatic contents of CE and FC are associated with increased number of WMH

No associations were found between hepatic DAG concentrations and brain parameters (Table 4 and Supplementary Table S4). In the crude model, TG and FC contents were associated with sCoV in temporal cortex and TG content was additionally associated with WMH count. These relationships were lost after adjustments of general characteristics (i.e. age, sex). By contrast, CE and FC concentrations showed significant positive associations with WMH count in all models.

Altogether, these linear regression analyses revealed three robust positive associations that remained significant in all models, namely between liver fibrosis and NAcc sCoV and between both liver FC and CE and WMH count.

3.4. NAcc sCoV and WMH count are associated with the expression of hepatic genes involved in inflammation and cellular stress

Next, liver-brain relationships were investigated using liver transcriptomics to assess canonical pathways and biological processes. For the brain parameters, only NAcc sCoV and WMH count (Fig. 2A-B, Supplementary video S1) were considered as they were associated with liver pathology in all linear regression models. Correlations were performed between liver gene expression and NAcc sCoV or WMH count datasets and the genes with significantly-correlating expression were used as input for pathway enrichment analysis. Significantly enriched canonical pathways and upstream regulators are displayed in Fig. 2 and Supplementary Tables S5-S8. Fibrogenic pathways, including 'Hepatic Fibrosis Signaling' and 'Actin Cytoskeleton Signaling', and the metabolic pathways 'GP6 Signaling' and 'HGF Signaling' were enriched with genes correlating with NAcc sCoV (Fig. 2C). Also pathogenic pathways related to more advanced stages of MASLD (e.g. 'Tumor Microenvironment') were identified with genes correlating with NAcc sCoV. Inflammatory pathways (e.g. 'TREM1 Signaling', 'Natural Killer Cell Signaling', 'Neutrophil Extracellular Trap Signaling') were also significantly enriched with genes correlating with NAcc sCoV. Consistently, the upstream regulator analysis showed associations between the predicted activation of inflammatory cytokines (including interferon-γ (IFNG), transforming growth factor-β1 (TGFB1), IL-1β (IL1B) and -18 (IL18) and tumor necrosis factor (TNF)) and NAcc sCoV (Fig. 2E). A parallel analysis of genes correlating with WMH count revealed canonical pathways related to cell cycle control and cellular stress (e.g. 'p53 Signaling', 'DNA damage-induced 14-3-3 sigma Signaling', upstream regulator tumor protein p53 (TP53)), pathways linked to metabolism control, mitochondrial dysfunction and neurodegeneration (e.g. 'Aryl Hydrocarbon Receptor Signaling' (AhR), 'TR/RXR activation' and 'BEX2 Signaling'), and an upstream regulator of mitochondrial function, 'calcium/calmodulin dependent protein kinase 2' (CAMKK2) (Fig. 2D and F).

Supplementary data related to this article can be found online at https://doi.org/10.1016/j.heliyon.2024.e38516

3.5. Higher NAcc sCoV is associated with increased circulating levels of IL-6

Liver NGS analyses revealed associations between the activation of inflammatory pathways, including IL- 1β and TNF with NAcc sCoV. To explore whether these relationships are reflected in the circulation, additional linear regressions were performed between plasma inflammatory markers (cytokines, acute phase proteins, complement factors) and NAcc sCoV (Table 5). Plasma concentrations of IL-6, a cytokine induced by IL- 1β and TNF- α , were significantly associated with higher NAcc sCoV in all models while the other inflammatory markers measured were not associated with NAcc sCoV.

Intrahepatic contents of CE and FC were associated with WMH count but no associations were found between WMH count and factors in plasma related to cholesterol metabolism (i.e. LDL-cholesterol, HDL-cholesterol and ApoB100, Supplementary Table S9).

To further identify potential molecular links between liver function and brain, plasma bile acid concentrations and fatty acids

 Table 4

 Significant associations between liver lipids and brain parameters.

Brain parameter	TG		DAG		CE		FC	
	β	P	β	P	β	P	β	P
sCoV								
Temporal cortex								
Crude model	0.006	0.008	-0.002	0.243	0.072	0.012	0.135	0.007
Full model	0.003	0.183	-0.002	0.330	0.048	0.098	0.073	0.198
Full $model + BMI$	0.004	0.148	-0.001	0.477	0.047	0.099	0.076	0.180
Full model $+$ T2DM	0.005	0.060	-0.002	0.282	0.066	0.027	0.102	0.078
$Full\ model + HT$	0.005	0.068	-0.001	0.488	0.061	0.037	0.087	0.124
WMH number								
Crude model	0.099	0.003	-0.036	0.119	1.404	0.000	2.437	0.001
Full model	0.090	0.018	-0.033	0.161	1.356	0.001	2.742	0.001
Full $model + BMI$	0.094	0.015	-0.030	0.210	1.353	0.001	2.773	0.001
Full model $+$ T2DM	0.091	0.026	-0.032	0.177	1.390	0.002	2.793	0.001
Full model + HT	0.092	0.023	-0.038	0.116	1.381	0.002	2.737	0.001

Results of linear regressions: Crude model: no adjustments; Full model: adjustment for age, sex, smoking, alcohol consumption and education; Full model + BMI: adjustment of full model + BMI: adjustment of full model + HT: adjustment of full model + hypertension. Full model + WC was additionally and exploratively tested and significant associations were similar to the ones observed in the Full model. Significant associations ($P \le 0.01$) are indicated in bold. Abbreviations: (CE) cholesteryl esters; (DAG) diacylglycerols; (FC) free cholesterol; (sCoV) spatial coefficient of variation; (TG) triglycerides; (WMH) white matter hyperintensities.

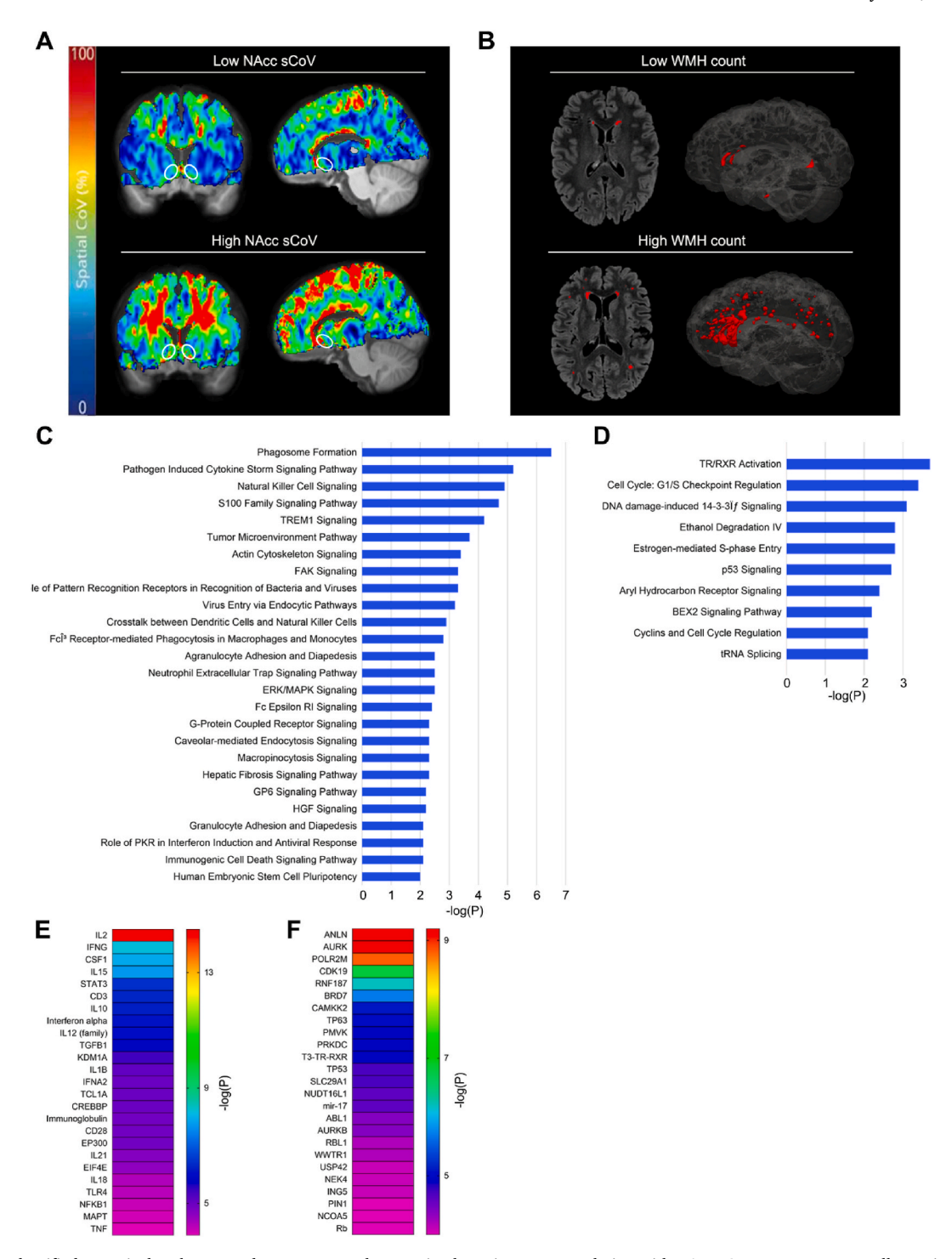


Fig. 2. Identified canonical pathways and upstream regulators using hepatic genes correlating with NAcc sCoV or WMH count. Illustrative picture depicting (A) low and high NAcc sCoV (average of n=6 participants each), and (B) low and high WMH count (n=1 representative participant each, for the complete 3D view see video S1). Hepatic genes of which the expression correlated respectively with NAcc sCoV or WMH count were used as input for pathway enrichment analysis. Significantly enriched canonical pathways in the liver ($\log(p\text{-value}) \ge 2$) for (C) NAcc sCoV and (D) WMH count. Top-25 liver upstream regulators enriched for (E) NAcc sCoV and (F) WMH count.

concentrations (determined in red blood cells) were analyzed. Neither bile acids nor fatty acids were found to be associated with NAcc sCoV or WMH count (Supplementary Tables S10–S11) indicating that these factors are unlikely to mediate the observed associations between liver and brain.

4. Discussion

This study investigated potential relationships between liver and brain health using comprehensive analyses of liver biopsies, neuroimaging and neuropsychological tests. The participants had obesity and exhibited MASLD characterized by pronounced steatosis and modest levels of inflammation and fibrosis which is consistent with other BS studies [51]. We did not find any associations between the mild liver pathology observed in this population and cognitive performance yet, which is consistent with previous research indicating that MASLD is associated with poorer cognitive performance mainly at more advanced stages of liver disease (reviewed in Ref. [16]) but not at early stages [14]. In line with this, we did not find any associations between liver parameters and MSMD, a marker of white matter integrity which is tightly linked to CSVD and cognition [52]. This may partly be explained by the absence of cognitive impairment in this study population as only early signs of neurodegeneration could be observed (e.g. very low amounts of WMH). However, we did already find associations between liver histopathology and cerebrovascular parameters: early liver fibrosis was associated with higher NAcc sCoV independent of age, sex, BMI, diabetes and hypertension. Higher sCoV reflects increased variations in CBF (decreased vascular efficiency) revealing early very subtle microvascular pathology. sCoV is notably associated with early stage of CSVD and cognitive impairment [35,53], suggesting that the population of the present study therefore exhibits only very early signs

Table 5Associations between plasma inflammatory markers and NAcc sCoV.

	NAcc sCoV						
	β	P	CI (95 %)				
CRP							
Crude model	-0.023	0.746	[-0.168; 0.121]				
Full model	-0.028	0.700	[-0.173; 0.117]				
Full model + BMI	-0.034	0.656	[-0.184; 0.117]				
Full model + T2DM	-0.006	0.941	[-0.158; 0.147]				
Full model + HT	-0.026	0.726	[-0.176; 0.124]				
LPSBP							
Crude model	-0.193	0.623	[-0.973; 0.587]				
Full model	-0.405	0.294	[-1.171; 0.361]				
$Full\ model + BMI$	-0.409	0.294	[-1.183; 0.365]				
$Full\ model + T2DM$	-0.338	0.390	[-1.121; 0.445]				
Full model + HT	-0.405	0.306	[-1.190 ; 0.381]				
IL-6							
Crude model	0.904	0.000	[0.496 ; 1.312]				
Full model	0.879	0.000	[0.461; 1.297]				
$Full\ model + BMI$	0.887	0.000	[0.465 ; 1.309]				
Full model + T2DM	0.867	0.000	[0.433; 1.301]				
Full model + HT	0.884	0.000	[0.462; 1.306]				
IL-1β							
Crude model	-0.366	0.476	[-1.389 ; 0.656]				
Full model	-0.234	0.646	[-1.251; 0.782]				
$Full\ model + BMI$	-0.219	0.675	[-1.264 ; 0.825]				
Full $model + T2DM$	-0.229	0.652	[-1.245 ; 0.786]				
Full $model + HT$	-0.229	0.658	[-1.258; 0.801]				
Complement C3							
Crude model	-0.001	0.880	[-0.008; 0.007]				
Full model	-0.002	0.618	[-0.009; 0.005]				
$Full\ model + BMI$	-0.002	0.628	[-0.009; 0.006]				
Full model + T2DM	-0.002	0.619	[-0.009; 0.005]				
Full model $+$ HT	-0.002	0.633	[-0.009; 0.006]				
Complement C5							
Crude model	-0.043	0.208	[-0.109; 0.024]				
Full model	-0.082	0.014	[-0.147; -0.017]				
Full model + BMI	-0.083	0.015	[-0.149; -0.017]				
Full model + T2DM	-0.079	0.027	[-0.149; -0.009]				
Full model + HT	-0.086	0.013	[-0.154; -0.019]				
AGTL4							
Crude model	-0.004	0.120	[-0.009; 0.001]				
Full model	-0.004	0.062	[-0.009; 0.000]				
$Full\ model + BMI$	-0.004	0.060	[-0.009 ; 0.000]				
Full model + T2DM	-0.004	0.104	[-0.009; 0.001]				
Full model + HT	-0.004	0.065	[-0.009 ; 0.000]				

Results of linear regressions: Crude model: no adjustments; Full model: adjustment for age, sex, smoking, alcohol consumption and education; Full model + BMI: adjustment of full model + BMI; Full model + T2DM: adjustment of full model + diabetes; Full model + HT: adjustment of full model + hypertension. Full model + WC was additionally and exploratively tested and significant associations were similar to the ones observed in the Full model. Significant associations (P \leq 0.01) are indicated in bold. Abbreviations: (ANGPTL4) angiopoietin-like 4; (CI) confidence interval; (CRP) C-reactive protein; (LPSBP) lipopolysaccharide binding protein; (NAcc) nucleus accumbens; (sCoV) spatial coefficient of variation.

of cerebrovascular deterioration, which might intensify over time and result in future cognitive decline [54]. Interestingly, in our earlier study on the same population, a significant improvement in cognitive performance was observed two years after bariatric surgery which was notably accompanied by a stabilization of sCoV in certain brain regions (e.g. temporal lobe area) [55]. Our findings align with prior studies showing that MASLD is related to disturbed brain blood perfusion [12,14,15]. The NAcc is part of the mesolimbic system which is involved in the reward system, and its activation has been notably related to the choice between immediate and delayed rewards implicated in hedonic feeding [56]. To substantiate our observations using an independent approach (NGS) and delineate the biological processes that may underlie this relationship, hepatic gene transcripts correlating with NAcc sCoV were analyzed on the level of pathways and upstream regulator activation. This analysis consistently identified pathways implicated in fibrosis development and immune responses pointing to sterile metabolic inflammation in combination with immune responses to pathogens. Numerous upstream cytokines with well-established roles in MASLD/fibrosis (e.g. IL-1β, IL-15, TNF-α, TGF-β) or immune response to pathogens (e.g. IL-2, IFN-γ) were predicted to be significantly activated and associated with NAcc sCoV. These findings together with the positive associations between plasma IL-6 concentrations and NAcc sCoV support the view that chronic inflammation may be involved in the relationship between liver fibrosis development and NAcc perfusion. It is possible that the liver affects brain function (IL-6 is produced by both Kupffer cells and hepatocytes [57]) or that both liver and brain simultaneously respond to external (circulating) signals. The liver is known to play an important role in obesity-associated chronic low-grade inflammation [58], as it can produce and secrete IL-6-inducible inflammatory proteins that can interact with the brain or adversely affect vasculature health [59]. Noteworthily, the morphology of omental white adipose tissue – which is also well-known to actively induce obesity-related systemic inflammation and is located in close anatomical proximity to the liver, was similarly positively associated with NAcc sCoV [18]. Altogether these findings suggest that systemic inflammatory molecules like IL-6 may mediate the relationships between liver and cerebrovascular health. The rationale for future therapeutic strategies to reduce IL-6-mediated inflammation is supported by our recent findings showing that individuals who cognitively improved upon BS were characterized by reduced plasma concentrations of leptin and CRP [43]. While leptin secretion from adipose tissue is mediated by IL-6, CRP is a strictly liver-derived protein that is primarily under control of IL-6 and IL-1\beta [60,61].

We also found associations between hepatic CE and FC contents and WMH count independently of age, sex, BMI, diabetes or hypertension. WMH of presumed vascular origin are areas presenting variable degrees of demyelination, axonal loss and neuroinflammation and are indicators of CSVD [7,62]. Previous studies reported that WMH volume was not associated with MASLD [63], but was associated with NASH or fibrosis [15]. It is important to note that in the present study population overall WMH burden was very low, which could explain why associations were mainly found with WMH count rather than volume since this metric reflects the absolute number of detrimental events of early WM deterioration. The observed association between both CE and FC and WMH count suggests that a common underlying disturbance in cholesterol homeostasis (e.g. high rate of cholesterol synthesis or reduced formation of cholesterol-derivatives) is related to cerebrovascular health. Under homeostatic conditions, a surplus of FC is neutralized enzymatically: CEs are formed from FC and fatty acids thereby preventing cytotoxic effects of FC that may lead to cellular and mitochondrial damage or sterile inflammation and ultimately promote liver pathologies like fibrosis and cancer [64]. Liver NGS analyses supported this, identifying critical pathways including cell cycle control, DNA damage, p53 signaling, ethanol breakdown and AhR signaling, the latter playing a role in cell proliferation and death, and carcinogenesis [65]. Plasma concentrations of LDL-cholesterol, HDL-cholesterol, ApoB100 or bile acids were not associated with WMH count implying that interindividual differences in hepatic cholesterol homeostasis are not directly reflected in the circulation at the level of lipoproteins themselves or particle numbers (represented by ApoB100). It is also possible that the turnover of circulating molecules derived from hepatic cholesterol is too dynamic in the circulation (e.g. uptake by other organs), and the assessment of their fluxes may be more critical for brain health than steady-state concentrations of lipoprotein particles and metabolites (lipids, bile acids) determined herein. Another possibility is that the liver – as a consequence of FC-induced inflammation and cellular damage - releases other inflammatory molecules that directly or indirectly affect cerebrovascular health.

It is noteworthy to highlight that the participants in this study, although being morbid obese, exhibited mostly early-stage MASLD and mild structural changes in the brain. This allowed us to identify associations between liver pathology and detrimental pathological changes in cerebrovascular function early in time (i.e. before cognitive dysfunction can be observed) which might then still be reversible. One of the major strengths of this study is the availability of relatively large wedge liver biopsies allowing histological but also biochemical and transcriptomics analyses. Typically, liver tissue is scarce (needle-biopsies) and MASLD parameters are often more indirectly evaluated using non-invasive techniques (e.g. blood markers, ultrasound, computed tomography [11,12,14]). In addition, extensive brain MRI was performed including novel biomarkers for grey and white matter integrity (e.g. MSMD, cortical thickness) and cerebrovascular health (e.g. sCoV, MSMD). Another strength is the relatively short time interval between MRI acquisition and the collection of liver biopsies (4–8 weeks). This is also a logistical challenge that resulted in the limitation of a cohort of relatively small size. One of the strengths of this study are the extensive datasets of metabolites (e.g. fatty acids, bile acids) and inflammatory proteins (e.g. cytokines, CRP). The availability of plasma that was collected at the time point of MRI notably allowed the identification of potential molecular mediators that can signal between liver and brain. However, many of these metabolites and proteins have high fluxes and low plasma half-lives and it is possible that other techniques (flux studies with micro-tracers) are necessary to identify more refined mediators. Another limitation is the cross-sectional nature of the study which prevents drawing conclusions regarding causality, and the lack of a healthy control group (for ethical reasons). Furthermore, females are overrepresented in this cohort and the inclusion of more males would allow greater generalization of the observed associations. However, the high number of female participants does reflect the typical population undergoing bariatric surgery in general (~80 % females) [66], and Roux-en-Y gastric bypass surgery specifically [67]. Besides, CBF measurements were corrected for partial volume but not for hematocrit values. Although hematocrit level did not correlate with CBF in the present study, it would have been appropriate to also correct CBF values for

hematocrit levels as the latter may influence T1-relaxation time of blood [68]. Another limitation is that we had to use BMI in our models to adjust for global obesity although the use of WC would have been more suitable to adjust for abdominal adiposity and metabolic comorbidities. The study was however performed during Covid-19 pandemic and WC was missing for \sim 20 % of the study population due to Covid-19 restrictions.

In conclusion, in middle-aged patients with obesity and predominantly mild MASLD (steatosis), liver histopathology and liver lipids are already associated with detrimental effects on cerebrovascular health independently of age, sex, BMI and metabolic comorbidities (diabetes and hypertension). These findings highlight the need for future research to focus on the onset of obesity-induced changes in the brain, even when changes in cognitive performance are not yet noticeable, and encourage future therapeutic strategies that aim to normalize metabolic-inflammatory aberrations that underlie obesity.

Data availability

The datasets generated and/or analyzed during the current study are available from the corresponding authors upon request. Liver RNAseq data is available in the Gene Expression Omnibus (GEO) repository (https://www.ncbi.nlm.nih.gov/gds); accession number: GSE249997.

Financial support

This work is supported by a grant of the Rijnstate-Radboudumc promotion fund. The histopathological and biochemical analyses were performed by the Netherlands Organisation for Applied Scientific Research (TNO) Metabolic Health Research (Leiden, the Netherlands) with support from TNO's Research program 'Brain Health', the seed Early Research Project 'Brain Power' and the Shared Research Program GLoBAL, an initiative of Radboudumc, Rijnstate and TNO.

Ethics statement

The study was conducted in compliance with the Declaration of Helsinki 'Ethical Principles for Medical Research Involving Human Subjects' and the guidelines for Good Clinical Practice (CPMP/ICH/135/95),. The BARICO study was approved by the medical review ethics committee CMO Region Arnhem and Nijmegen (NL63493.091.17) and prospectively registered in the Dutch Trial Registry [19].

CRediT authorship contribution statement

Florine Seidel: Writing – review & editing, Writing – original draft, Investigation, Formal analysis. Debby Vreeken: Writing – review & editing, Investigation, Formal analysis. Emma Custers: Writing – review & editing, Investigation. Maximilian Wiesmann: Writing – review & editing, Writing – original draft, Formal analysis. Serdar Özsezen: Writing – review & editing, Formal analysis, Data curation. Wim van Duyvenvoorde: Writing – review & editing, Investigation, Data curation. Martien Caspers: Writing – review & editing, Software, Data curation. Aswin Menke: Writing – review & editing, Formal analysis. Martine C. Morrison: Writing – review & editing, Writing – original draft. Lars Verschuren: Writing – review & editing, Formal analysis. Marco Duering: Writing – review & editing, Resources. Eric J. Hazebroek: Writing – review & editing, Resources, Methodology, Conceptualization. Amanda J. Kiliaan: Writing – review & editing, Writing – original draft, Methodology, Funding acquisition, Formal analysis, Conceptualization. Robert Kleemann: Writing – review & editing, Writing – original draft, Methodology, Funding acquisition, Formal analysis, Conceptualization.

Declaration of competing interest

The authors declare that they have no known competing financial interests or personal relationships that could have appeared to influence the work reported in this paper.

Acknowledgements

The authors thank A. Hofboer for her contribution on participant recruitment and data collection as well as T.J. Aufenacker and B. P.L. Witteman for collecting the liver biopsies.

Appendix A. Supplementary data

Supplementary data to this article can be found online at https://doi.org/10.1016/j.heliyon.2024.e38516.

References

[1] H. Tanaka, D.D. Gourley, M. Dekhtyar, A.P. Haley, Cognition, brain structure, and brain function in individuals with obesity and related disorders, Curr. Obes. Rep. 9 (2020) 544–549. https://doi.org/10.1007/s13679-020-00412-y

- [2] I.A.C. Arnoldussen, D.R. Gustafson, E.M.C. Leijsen, F.E. de Leeuw, A.J. Kiliaan, Adiposity is related to cerebrovascular and brain volumetry outcomes in the RUN DMC study, Neurology 93 (2019) e864–e878, https://doi.org/10.1212/WNL.0000000000000000000.
- [3] M. Hamer, G.D. Batty, Association of body mass index and waist-to-hip ratio with brain structure: UK Biobank study, Neurology 92 (2019) e594–e600, https://doi.org/10.1212/WNL.0000000000006879.
- [4] M.E. Shaw, P.S. Sachdev, W. Abhayaratna, K.J. Anstey, N. Cherbuin, Body mass index is associated with cortical thinning with different patterns in mid- and late-life, Int. J. Obes. 42 (2018) 455–461, https://doi.org/10.1038/ijo.2017.254.
- [5] Y.-S. Qiao, X. Tang, Y.-H. Chai, H.-J. Gong, H. Xu, I. Patel, L. Li, T. Lu, W.-Y. Zhao, Z.-Y. Li, M.A. Cardoso, J.-B. Zhou, Cerebral blood flow alterations and obesity: a systematic review and meta-analysis. J. Alzheimer's Dis. (2022) 1–17. https://doi.org/10.3233/jad-220601.
- [6] L. Lampe, R. Zhang, F. Beyer, S. Huhn, S. Kharabian Masouleh, S. Preusser, P.L. Bazin, M.L. Schroeter, A. Villringer, A.V. Witte, Visceral obesity relates to deep white matter hyperintensities via inflammation, Ann. Neurol. 85 (2019) 194–203, https://doi.org/10.1002/ana.25396.
- [7] J.M. Wardlaw, E.E. Smith, G.J. Biessels, C. Cordonnier, F. Fazekas, R. Frayne, R.I. Lindley, J.T. O'Brien, F. Barkhof, O.R. Benavente, S.E. Black, C. Brayne, M. Breteler, H. Chabriat, C. DeCarli, F.E. de Leeuw, F. Doubal, M. Duering, N.C. Fox, S. Greenberg, V. Hachinski, I. Kilimann, V. Mok, R. van Oostenbrugge, L. Pantoni, O. Speck, B.C.M. Stephan, S. Teipel, A. Viswanathan, D. Werring, C. Chen, C. Smith, M. van Buchem, B. Norrving, P.B. Gorelick, M. Dichgans, Neuroimaging standards for research into small vessel disease and its contribution to ageing and neurodegeneration, Lancet Neurol. 12 (2013) 822–838, https://doi.org/10.1016/S1474-4422(13)70124-8.
- [8] R.A. Charlton, T.R. Barrick, D.J. McIntyre, Y. Shen, M. O'Sullivan, F.A. Howe, C.A. Clark, R.G. Morris, H.S. Markus, White matter damage on diffusion tensor imaging correlates with age-related cognitive decline, Neurology 66 (2006) 217–222, https://doi.org/10.1212/01.wnl.0000194256.15247.83.
- [9] J. Daoust, J. Schaffer, Y. Zeighami, A. Dagher, I. García-García, A. Michaud, White matter integrity differences in obesity: a meta-analysis of diffusion tensor imaging studies, Neurosci. Biobehav. Rev. 129 (2021) 133–141, https://doi.org/10.1016/j.neubiorev.2021.07.020.
- [10] D.A. Bender, Introduction to Nutrition and Metabolism, 2014.
- [11] L.B. VanWagner, J.G. Terry, L.S. Chow, A.C. Alman, H. Kang, K.H. Ingram, C. Shay, C.E. Lewis, R.N. Bryan, L.J. Launer, J. Jeffrey Carr, Nonalcoholic fatty liver disease and measures of early brain health in middle-aged adults: the CARDIA study, Obesity 25 (2017) 642–651, https://doi.org/10.1002/oby.21767.
- [12] G. Weinstein, S. Zelber-Sagi, S.R. Preis, A.S. Beiser, C. DeCarli, E.K. Speliotes, C.L. Satizabal, R.S. Vasan, S. Seshadri, Association of nonalcoholic fatty liver disease with lower brain volume in healthy middle-aged adults in the Framingham Study, JAMA Neurol. 75 (2018) 97–104, https://doi.org/10.1001/jamaneurol.2017.3229.
- [13] L. Airaghi, M. Rango, D. Maira, V. Barbieri, L. Valenti, R. Lombardi, P. Biondetti, S. Fargion, A.L. Fracanzani, Subclinical cerebrovascular disease in NAFLD without overt risk factors for atherosclerosis, Atherosclerosis 268 (2018) 27–31, https://doi.org/10.1016/j.atherosclerosis.2017.11.012.
- [14] P. Yilmaz, L.J.M. Alferink, L.G.M. Cremers, S.D. Murad, W.J. Niessen, M.A. Ikram, M.W. Vernooij, Subclinical liver traits are associated with structural and hemodynamic brain imaging markers, Liver Int. 43 (2023) 1256–1268, https://doi.org/10.1111/liv.15549.
- [15] S. Petta, A. Tuttolomondo, C. Gagliardo, R. Zafonte, G. Brancatelli, D. Cabibi, C. Camma, V. Di Marco, L. Galvano, G. La Tona, A. Licata, F. Magliozzo, C. Maida, G. Marchesini, G. Merlino, M. Midiri, G. Parrinello, D. Torres, A. Pinto, A. Craxi, The presence of white matter lesions is associated with the fibrosis severity of nonalcoholic fatty liver disease, Med 95 (2016) 1–8, https://doi.org/10.1097/MD.000000000003446. United States).
- [16] K. Kjærgaard, A.C.D. Mikkelsen, C.W. Wernberg, L.L. Grønkjær, P.L. Eriksen, M.F. Damholdt, R.P. Mookerjee, H. Vilstrup, M.M. Lauridsen, K.L. Thomsen, Cognitive dysfunction in non-alcoholic fatty liver disease—current knowledge, mechanisms and perspectives, J. Clin. Med. 10 (2021) 1–20, https://doi.org/10.3390/jcm10040673.
- [17] D. Vreeken, M. Wiesmann, L.N. Deden, I.A.C. Arnoldussen, E. Aarts, R.P.C. Kessels, R. Kleemann, E.J. Hazebroek, E.O. Aarts, A.J. Kiliaan, Study rationale and protocol of the BARICO study: a longitudinal, prospective, observational study to evaluate the effects of weight loss on brain function and structure after bariatric surgery, BMJ Open 9 (2019) 1–8, https://doi.org/10.1136/bmjopen-2018-025464.
- [18] D. Vreeken, F. Seidel, G. de la Roij, W. Vening, W. den Hengst, L. Verschuren, S. Özsezen, R.P.C. Kessels, M. Duering, H.J.M.M. Mutsaerts, R. Kleemann, M. Wiesmann, E.J. Hazebroek, A.J. Kiliaan, Impact of white adipose tissue on brain structure, perfusion and cognitive function in patients with severe obesity: the BARICO study, Neurology (2022), https://doi.org/10.1212/WNL.0000000000201538.
- [19] Landelijk Trial Register. The effects ofweight loss after bariatric surgery on brain function and structure., (n.d.). https://onderzoekmetmensen.nl/en/trial/28949 (accessed June 7, 2024).
- [20] B. Fischl, A.M. Dale, Measuring the thickness of the human cerebral cortex from magnetic resonance images, Proc. Natl. Acad. Sci. U. S. A. 97 (2000) 11050–11055, https://doi.org/10.1073/pnas.200033797.
- [21] R.S. Desikan, F. Ségonne, B. Fischl, B.T. Quinn, B.C. Dickerson, D. Blacker, R.L. Buckner, A.M. Dale, R.P. Maguire, B.T. Hyman, M.S. Albert, R.J. Killiany, An automated labeling system for subdividing the human cerebral cortex on MRI scans into gyral based regions of interest, Neuroimage 31 (2006) 968–980, https://doi.org/10.1016/j.neuroimage.2006.01.021.
- [22] J. Mazziotta, A. Toga, A. Evans, P. Fox, J. Lancaster, K. Zilles, R. Woods, T. Paus, G. Simpson, B. Pike, C. Holmes, L. Collins, P. Thompson, D. MacDonald, M. Iacoboni, T. Schormann, K. Amunts, N. Palomero-Gallagher, S. Geyer, L. Parsons, K. Narr, N. Kabani, G. Le Goualher, D. Boomsma, T. Cannon, R. Kawashima, B. Mazoyer, A probabilistic atlas and reference system for the human brain: international Consortium for Brain Mapping (ICBM), Philos. Trans. R. Soc. B Biol. Sci. 356 (2001) 1293–1322, https://doi.org/10.1098/rstb.2001.0915.
- [23] B. Vogt (Ed.), Cingulate Neurobiology and Disease, Oxford University Press, 2009.
- [24] L.Q. Uddin, J.S. Nomi, B. Hébert-Seropian, J. Ghaziri, O. Boucher, Structure and function of the human insula, J. Clin. Neurophysiol. 34 (2017) 300–306, https://doi.org/10.1097/WNP.0000000000000377.
- [25] S.H. Chao, Y.T. Liao, V.C.H. Chen, C.J. Li, R.S. McIntyre, Y. Lee, J.C. Weng, Correlation between brain circuit segregation and obesity, Behav. Brain Res. 337 (2018) 218–227, https://doi.org/10.1016/j.bbr.2017.09.017.
- [26] M.J. Herrmann, A.K. Tesar, J. Beier, M. Berg, B. Warrings, Grey matter alterations in obesity: a meta-analysis of whole-brain studies, Obes. Rev. 20 (2019) 464–471, https://doi.org/10.1111/obr.12799.
- [27] K. Braunlich, C. Seger, The basal ganglia, Wiley Interdiscip. Rev. Cogn. Sci. 4 (2013) 135-148, https://doi.org/10.1002/wcs.1217.
- [28] Z. Tan, Y. Hu, G. Ji, G. Li, Y. Ding, W. Zhang, J. Wang, Z. Jia, L. Zhang, H. Li, K.M. von Deneen, Y. Han, G. Cui, P. Manza, N.D. Volkow, Y. Nie, G.J. Wang, Y. Zhang, Alterations in functional and structural connectivity of basal ganglia network in patients with obesity, Brain Topogr. 35 (2022) 453–463, https://doi.org/10.1007/s10548-022-00906-z.
- [29] M.S. Izadi, M. Radahmadi, Overview of the central amygdala role in feeding behaviour, Br. J. Nutr. 127 (2022) 953–960, https://doi.org/10.1017/ S0007114521002312.
- [30] G. Šimić, M. Tkalčić, V. Vukić, D. Mulc, E. Španić, M. Šagud, F.E. Olucha-Bordonau, M. Vukšić, P.R. Hof, Understanding emotions: origins and roles of the amygdala, Biomolecules 11 (2021) 1–58, https://doi.org/10.3390/biom11060823.
- [31] P. Andersen, R. Morris, D. Amaral, T. Bliss, J. O'Keefe, The Hippocampus Book, Oxford University Press, 2006, https://doi.org/10.1093/acprof:oso/9780195100273.001.0001.
- [32] H.J.M.M. Mutsaerts, J. Petr, P. Groot, P. Vandemaele, S. Ingala, A.D. Robertson, L. Václavů, I. Groote, H. Kuijf, F. Zelaya, O. O'Daly, S. Hilal, A.M. Wink, I. Kant, M.W.A. Caan, C. Morgan, J. de Bresser, E. Lysvik, A. Schrantee, A. Bjørnebekk, P. Clement, Z. Shirzadi, J.P.A. Kuijer, V. Wottschel, U.C. Anazodo, D. Pajkrt, E. Richard, R.P.H. Bokkers, L. Reneman, M. Masellis, M. Günther, B.J. MacIntosh, E. Achten, M.A. Chappell, M.J.P. van Osch, X. Golay, D.L. Thomas, E. De Vita, A. Bjørnerud, A. Nederveen, J. Hendrikse, I. Aslani, F. Barkhof, ExploreASL: an image processing pipeline for multi-center ASL perfusion MRI studies, Neuroimage 219 (2020), https://doi.org/10.1016/j.neuroimage.2020.117031.

[33] I. Asllani, A. Borogovac, T.R. Brown, Regression algorithm correcting for partial volume effects in arterial spin labeling MRI, Magn. Reson. Med. 60 (2008) 1362–1371, https://doi.org/10.1002/mrm.21670.

- [34] Z. Wang, Improving cerebral blood flow quantification for arterial spin labeled perfusion MRI by removing residual motion artifacts and global signal fluctuations, Magn. Reson. Imaging 30 (2012) 1409–1415, https://doi.org/10.1016/j.mri.2012.05.004.
- [35] H.J.M.M. Mutsaerts, J. Petr, L. Václavů, J.W. van Dalen, A.D. Robertson, M.W. Caan, M. Masellis, A.J. Nederveen, E. Richard, B.J. MacIntosh, The spatial coefficient of variation in arterial spin labeling cerebral blood flow images, J. Cerebr. Blood Flow Metabol. 37 (2017) 3184–3192, https://doi.org/10.1177/0271678X16683690.
- [36] S. Andermatt, S. Pezold, P.C. Cattin, Automated segmentation of multiple sclerosis lesions using multi-dimensional gated recurrent units, 31-42, https://doi.org/10.1007/978-3-319-75238-9 3, 2018.
- [37] S.M. Smith, M. Jenkinson, M.W. Woolrich, C.F. Beckmann, T.E.J. Behrens, H. Johansen-Berg, P.R. Bannister, M. De Luca, I. Drobnjak, D.E. Flitney, R.K. Niazy, J. Saunders, J. Vickers, Y. Zhang, N. De Stefano, J.M. Brady, P.M. Matthews, Advances in functional and structural MR image analysis and implementation as FSL, Neuroimage 23 (2004) 208–219, https://doi.org/10.1016/j.neuroimage.2004.07.051.
- [38] F. Verhage, Intelligentie en leeftijd bij volwassenen en bejaarden, Van Gorcum, 1964.
- [39] W. D., Adult Intelligence Scale-Fourth Edition (WAIS-IV), 2008.
- [40] B.A. Wilson, J. Cockburn, A.D. Baddeley, The Rivermead Behavioural Memory Test, 1991.
- [41] B. Schmand, S.C. Groenink, M. den Dungen, Letterfluency: psychometrische eigenschappen en Nederlandse normen, Tijdschr Gerontol. Geriatr. 39 (2008) 64–74, https://doi.org/10.1007/BF03078128.
- [42] Z. Pg, F. B, Exercise care in using UAP (unlicensed assistive personnel): a cautionary tale Title, Manag 7 (1995) 76–77.
- [43] D. Vreeken, F. Seidel, E.M. Custers, L. Olsthoorn, S. Cools, E.O. Aarts, R. Kleemann, R.P.C. Kessels, M. Wiesmann, E.J. Hazebroek, A.J. Kiliaan, Factors associated with cognitive improvement after bariatric surgery among patients with severe obesity in The Netherlands, JAMA Netw. Open 6 (2023) e2315936, https://doi.org/10.1001/jamanetworkopen.2023.15936.
- [44] D.E. Kleiner, E.M. Brunt, M. Van Natta, C. Behling, M.J. Contos, O.W. Cummings, L.D. Ferrell, Y.C. Liu, M.S. Torbenson, A. Unalp-Arida, M. Yeh, A. J. McCullough, A.J. Sanyal, Design and validation of a histological scoring system for nonalcoholic fatty liver disease, Hepatology 41 (2005) 1313–1321, https://doi.org/10.1002/hep.20701.
- [45] M. Hjelkrem, C. Stauch, J. Shaw, S.A. Harrison, Validation of the non-alcoholic fatty liver disease activity score, Aliment. Pharmacol. Ther. 34 (2011) 214–218, https://doi.org/10.1111/j.1365-2036.2011.04695.x.
- [46] W. Liang, A.L. Menke, A. Driessen, G.H. Koek, J.H. Lindeman, R. Stoop, L.M. Havekes, R. Kleemann, A.M. Van Den Hoek, Establishment of a general NAFLD scoring system for rodent models and comparison to human liver pathology, PLoS One 9 (2014) 1–17, https://doi.org/10.1371/journal.pone.0115922.
- [47] A.M. Mueller, R. Kleemann, E. Gart, W. van Duyvenvoorde, L. Verschuren, M. Caspers, A. Menke, N. Krömmelbein, K. Salic, Y. Burmeister, B. Seilheimer, M. C. Morrison, Cholesterol accumulation as a driver of hepatic inflammation under translational dietary conditions can Be attenuated by a multicomponent medicine, Front. Endocrinol. 12 (2021) 1–14, https://doi.org/10.3389/fendo.2021.601160.
- [48] K. Salic, E. Gart, F. Seidel, L. Verschuren, M. Caspers, W. van Duyvenvoorde, K.E. Wong, J. Keijer, I. Bobeldijk-Pastorova, P.Y. Wielinga, R. Kleemann, Combined treatment with L-carnitine and nicotinamide riboside improves hepatic metabolism and attenuates obesity and liver steatosis, Int. J. Mol. Sci. 20 (2019) 1–16, https://doi.org/10.3390/ijms20184359.
- [49] M.C. Morrison, E. Gart, W. van Duyvenvoorde, J. Snabel, M.J. Nielsen, D.J. Leeming, A. Menke, R. Kleemann, Heat-inactivated akkermansia muciniphila improves gut permeability but does not prevent development of non-alcoholic steatohepatitis in diet-induced obese Ldlr—/—.Leiden mice, Int. J. Mol. Sci. 23 (2022) 1–17. https://doi.org/10.3390/jims23042325.
- [50] E. Gart, K. Salic, M.C. Morrison, M. Caspers, W. van Duyvenvoorde, M. Heijnk, M. Giera, I. Bobeldijk-Pastorova, J. Keijer, A.B. Storsve, P.A. Hals, R. Kleemann, Krill oil treatment increases distinct pufas and oxylipins in adipose tissue and liver and attenuates obesity-associated inflammation via direct and indirect mechanisms, Nutrients 13 (2021), https://doi.org/10.3390/nu13082836.
- [51] M. Machado, P. Marques-Vidal, H. Cortez-Pinto, Hepatic histology in obese patients undergoing bariatric surgery, J. Hepatol. 45 (2006) 600–606, https://doi.org/10.1016/j.jhep.2006.06.013.
- [52] E. Baykara, B. Gesierich, R. Adam, A.M. Tuladhar, J.M. Biesbroek, H.L. Koek, S. Ropele, E. Jouvent, H. Chabriat, B. Ertl-Wagner, M. Ewers, R. Schmidt, F. de Leeuw, G.J. Biessels, M. Dichgans, M. Duering, A novel imaging marker for small vessel disease based on skeletonization of white matter tracts and diffusion histograms, Ann. Neurol. 80 (2016) 581–592, https://doi.org/10.1002/ana.24758.
- [53] C.A. Morgan, T.R. Melzer, R.P. Roberts, K. Wiebels, H.J.M.M. Mutsaerts, M.J. Spriggs, J.C. Dalrymple-Alford, T.J. Anderson, N.J. Cutfield, G. Deib, J. Pfeuffer, D. R. Addis, I.J. Kirk, L.J. Tippett, Spatial variation of perfusion MRI reflects cognitive decline in mild cognitive impairment and early dementia, Sci. Rep. 11 (2021) 1–9, https://doi.org/10.1038/s41598-021-02313-z.
- [54] N. Mokhber, A. Shariatzadeh, A. Avan, H. Saber, G.S. Babaei, G. Chaimowitz, M.R. Azarpazhooh, Cerebral blood flow changes during aging process and in cognitive disorders: a review, NeuroRadiol. J. 34 (2021) 300–307, https://doi.org/10.1177/19714009211002778.
- [55] E. Custers, D. Vreeken, R. Kleemann, R.P.C. Kessels, M. Duering, J. Brouwer, T.J. Aufenacker, B.P.L. Witteman, J. Snabel, E. Gart, H.J.M.M. Mutsaerts, M. Wiesmann, E.J. Hazebroek, A.J. Kiliaan, Long-term brain structure and cognition following bariatric surgery, JAMA Netw. Open 7 (2024) E2355380, https://doi.org/10.1001/jamanetworkopen.2023.55380.
- [56] B.M. Appelhans, Neurobehavioral inhibition of reward-driven feeding: implications for dieting and obesity, Obesity 17 (2009) 640–647, https://doi.org/10.1038/oby.2008.638.
- [57] D. Schmidt-Arras, S. Rose-John, IL-6 pathway in the liver: from physiopathology to therapy, J. Hepatol. 64 (2016) 1403–1415, https://doi.org/10.1016/j. jhep.2016.02.004.
- [58] A.R. Saltiel, J.M. Olefsky, Inflammatory mechanisms linking obesity and metabolic disease, J. Clin. Invest. 127 (2017) 1-4, https://doi.org/10.1172/JCI92035.
- [59] N. Gehrke, J.M. Schattenberg, Metabolic inflammation—a role for hepatic inflammatory pathways as drivers of comorbidities in nonalcoholic fatty liver disease? Gastroenterology 158 (2020) 1929–1947.e6, https://doi.org/10.1053/j.gastro.2020.02.020.
- [60] S. Wueest, D. Konrad, The role of adipocyte-specific IL-6-type cytokine signaling in FFA and leptin release, Adipocyte 7 (2018) 226–228, https://doi.org/10.1080/21623945.2018.1493901.
- [61] R. Kleemann, P.P. Gervois, L. Verschuren, B. Staels, H.M.G. Princen, T. Kooistra, Fibrates down-regulate IL-1-stimulated C-reactive protein gene expression in hepatocytes by reducing nuclear p50-NFκβ-C/EΒΡ-β complex formation, Blood 101 (2003) 545–551, https://doi.org/10.1182/blood-2002-06-1762.
- [62] G. Solé-Guardia, E. Custers, A. de Lange, E. Clijncke, B. Geenen, J. Gutierrez, B. Küsters, J.A.H.R. Claassen, F.E. de Leeuw, M. Wiesmann, A.J. Kiliaan, Association between hypertension and neurovascular inflammation in both normal-appearing white matter and white matter hyperintensities, Acta Neuropathol. Commun 11 (2023) 1–12, https://doi.org/10.1186/s40478-022-01497-3.
- [63] G. Weinstein, K. Davis-Plourde, J.J. Himali, S. Zelber-Sagi, A.S. Beiser, S. Seshadri, Non-alcoholic fatty liver disease, liver fibrosis score and cognitive function in middle-aged adults: the Framingham Study, Liver Int. 39 (2019) 1713–1721, https://doi.org/10.1111/liv.14161.
- [64] C.L. Horn, A.L. Morales, C. Savard, G.C. Farrell, G.N. Ioannou, Role of cholesterol-associated steatohepatitis in the development of NASH, Hepatol. Commun. 6 (2022) 12–35, https://doi.org/10.1002/hep4.1801.
- [65] N.Y. Patil, J.E. Friedman, A.D. Joshi, Role of hepatic aryl Hydrocarbon receptor in non-alcoholic fatty liver disease, Receptors 2 (2023) 1–15, https://doi.org/10.3390/receptors2010001.
- [66] H.F. Fuchs, R.C. Broderick, C.R. Harnsberger, D.C. Chang, B.J. Sandler, G.R. Jacobsen, S. Horgan, Benefits of bariatric surgery do not reach obese men, J. Laparoendosc. Adv. Surg. Tech. 25 (2015) 196–201, https://doi.org/10.1089/lap.2014.0639.
- [67] J. Bal, N. Ilonzo, T. Adediji, I.M. Leitman, Gender as a deterministic factor in procedure selection and outcomes in bariatric surgery, J. Soc. Laparoendosc. Surg. 25 (2021) 1–9, https://doi.org/10.4293/JSLS.2020.00077.
- [68] P.W. Hales, F.J. Kirkham, C.A. Clark, A general model to calculate the spin-lattice (T1) relaxation time of blood, accounting for haematocrit, oxygen saturation and magnetic field strength, J. Cerebr. Blood Flow Metabol. 36 (2016) 370–374, https://doi.org/10.1177/0271678X15605856.